Seismic Performance of Reinforced Concrete Interior Beam-Column Joints with Novel Reinforcement Detail

Xinyu Shen[1], Bo Li[1,*], Yung-Tsang Chen[1], Walid Tizani[2]

[1] Department of Civil Engineering, University of Nottingham Ningbo China, Ningbo 315100, China
[2] Department of Civil Engineering, University of Nottingham, Nottingham NG7 2RD, UK
[*]Corresponding author: bo.li@nottingham.edu.cn

Abstract

Horizontal stirrups are normally required in reinforced concrete (RC) beam-column joints (BCJs) for resisting shear forces in seismic design. For RC moment-resisting frames subjected to a high lateral loading, a large number of stirrups are needed in joint cores. This may cause reinforcement congestion, leading to construction difficulty and insufficient concrete compaction, which can result in poor seismic performance. In this study, a novel reinforcement detail in the form of unbonded diagonal bars mechanically anchored at beam ends is proposed for RC interior BCJs. The detail alleviates the reinforcement congestion through partially replacing horizontal stirrups, and improves the seismic performance of BCJs by plastic hinge relocation and input shear force reduction mechanisms. Four 2/3-scale RC interior BCJ specimens were prepared and tested under quasi-static cyclic load, including one specimen designed with the current code and three specimens adopting the proposed reinforcement detail. Test results show that the proposed reinforcement detail is able to relocate the plastic hinges away from beam-joint interfaces as well as improve the loading capacity, energy dissipation capacity, stiffness, and bonding condition of beam reinforcements within the cores of BCJs. The combined use of stirrups and the proposed reinforcement detail significantly enhances the cracking resistance and reduces joint distortion, while additional amount of stirrups results in a marginal improvement. Moreover, an analytical model considering plastic hinge relocation and input joint shear force reduction is proposed for BCJs with the novel reinforcement detail. The model can adequately predict the failure mode and loading capacity of BCJ specimens.

Keywords: beam-column joints, seismic performance, diagonal bars, plastic hinge relocation, reinforced concrete.

1. Introduction

Reinforced concrete (RC) moment-resisting frame is a typical structural form, in which beam-column joints (BCJs) are defined as the parts of columns where transverse beams are connected. The BCJs play a crucial role in seismic design of structures as they transfer loads between beams and columns [1]. Under lateral action such as earthquakes, the shear force inside joint cores could be several times higher than that in the adjacent structural members [2]. Reconnaissance of previous earthquakes has indicated that the failure of BCJs could lead to large story drifts and even the global collapse of structures [3]. Nowadays BCJs have been recognized as critical structural components in frames, and current codes [4] specify the concept of “strong joint-weak members” in the design of moment-

resisting frames. Therefore, the BCJs must be properly designed and detailed to prevent their failure prior to beams or columns.

The shear resistance mechanism of BCJs is more complicated than that of beams and columns. Paulay *et al.* [5] proposed that the shear forces in BCJs are resisted through the truss and the diagonal concrete strut mechanisms. Horizontal stirrups are required to transfer forces in the truss mechanism, and sufficient sectional area and concrete strength are the main parameters affecting the force taken by the diagonal concrete strut mechanism. In addition, joint stirrups provide confinement to the concrete strut inside joint core and enhance the shear resistance of BCJs [6]. Consequently, a large quantity of stirrups may be required in BCJs, especially for those subjected to a large horizontal force, which brings about the problem of reinforcement congestion when the space of joint core is limited. As a result, construction difficulty and insufficient concrete compaction occur inside joint cores, leading to unsatisfactory seismic performance of BCJs.

Alternative reinforcements for BCJs have been developed to address the above-mentioned issues, such as diagonal bars. Tsonos *et al.* [7] found that RC exterior BCJs with diagonal bars are able to resist higher horizontal shear stress than those with conventional stirrups. Au *et al.* [8] compared the seismic behaviour of interior BCJs with no joint reinforcement, conventional stirrups and diagonal bars. It was found that the use of diagonal bars enhances the loading capacity of BCJs and improves the bond condition between longitudinal reinforcements and joint concrete. Chalioris *et al.* [9] compared the seismic performance of exterior BCJs with different reinforcement details. The BCJs with diagonal bars show higher loading capacity and energy dissipation capacity than those with or without conventional stirrups. The combined use of stirrups and diagonal bars inside joint core is recommended for crack control. Kotsovou and Mouzakis [10] found that the shear deformation of BCJs is significantly reduced when 80% of conventional stirrups are replaced with diagonal bars. Lu *et al.* [11] compared the seismic performance of interior BCJs with diagonal bars to those with conventional stirrups. Although those BCJs with diagonal bars exhibit enhanced loading capacity, the importance of confinement from stirrups in achieving ductile behaviour of BCJs is emphasized. Diagonal bars combined with hair clip bars were also developed as reinforcement for exterior BCJs [12,13]. The addition of diagonal bars to hair clip bars inside joint cores enhances the shear strength and overall loading capacity of BCJs without compromising their ductility and stiffness. Furthermore, several analytical models have been successfully developed for estimating the shear strength of BCJs with diagonal bars [14,15]. It has been demonstrated that the use of diagonal bars as joint reinforcement is effective in resisting shear forces in BCJs. Nevertheless, the diagonal bars bonded with joint concrete transferred the forces on diagonal bars into joint cores, which causes damage to joint concrete.

On the other hand, plastic hinge relocation has also been proposed to improve the seismic performance of BCJs. When plastic hinge is moved away from the beam-joint interface, yielding penetration of beam longitudinal bars into joint can be weakened, leading to a reduced joint shear action. Park and Milburn [16] and Hwang *et al.* [17] provided additional steel bars anchored in the beam ends for both exterior and interior BCJs, respectively. As a result, the plastic hinges in both types of joint were successfully relocated away from the beam-joint interfaces, which improves the bonding between beam longitudinal bars and joint concrete. Moreover, BCJs with relocated plastic hinges exhibit higher energy dissipation capacity and shear strength. To retrofit BCJs, CFRP sheets were bonded at the beam-joint interface for relocating plastic hinges [18,19]. The plastic hinges were relocated to the ends of CFRP sheets so that the joint failure could be prevented, resulting in higher loading capacity and

ductility of BCJs. Wang *et al.* [20] tested seismically deficient exterior BCJs retrofitted by externally bonded CFRP sheets and near-surface mounted CFRP strips. Both strengthening methods effectively relocated the plastic hinge away from the joint region and consequently protected the joint cores. In summary, the plastic hinge relocation is achieved mainly by enhancing flexural capacity of beam sections close to joint.

In this paper, a novel reinforcement detail in the form of diagonal bars with horizontal mechanical anchorage segments at beam ends is proposed for RC interior BCJs. The diagonal segments of the bars are covered with PVC tubes to prevent their bonding with joint concrete. The ends of anchorage segments are equipped with mechanical anchors (e.g. steel anchorage heads) to provide sufficient anchorage for diagonal bars and control the location of the plastic hinge of the beam through changing the reinforcement ratio along the beam. Relocation of the plastic hinge away from the beam-column interface is advantageous in relieving strength degradation in the joint due to strain penetration effect. To verify the effectiveness of using the proposed reinforcement detail to replace conventional stirrups, four 2/3-scale interior BCJ specimens, including one control specimen designed according to the Chinese code [4] and three specimens adopting the proposed reinforcement detail, were prepared and tested under quasi-static cyclic load. The influence of joint reinforcement detail (conventional stirrups or the proposed detail) and the quantity of joint stirrups on the seismic performance of interior BCJs is investigated. Furthermore, an analytical model is developed to predict the failure mode and loading capacity of BCJs with the proposed reinforcement detail.

2. Experimental programme

2.1 New reinforcement detail for BCJs

Figure 1 shows the conventional stirrups and the proposed reinforcement detail for a RC interior BCJ. The proposed reinforcement detail aims to partially replace stirrups in joint cores to alleviate the reinforcement congestion and enhance the seismic behaviour of RC BCJs. Moreover, the proposed reinforcement detail utilizes the unused space in joint so that it can also be combined with conventional horizontal stirrups. This reinforcement detail is developed based on the plastic hinge relocation and the joint shear force reduction mechanisms. To relocate plastic hinge, the flexural capacity of beam sections close to joint needs to be enhanced. This can be achieved by increasing reinforcement ratio at the beam ends through the presence of the anchorage segments of the proposed reinforcement detail. Senturk *et al.* [21] installed steel heads on the ends of reinforcement bars to enhance the connection between precast beam and column. They found that the steel heads are able to improve the anchorage between beam longitudinal bars and beam end plate. The idea is adopted in this study and steel heads are installed at the ends of the anchorage segments to improve the anchorage of diagonal bars and control the position of plastic hinges. The plastic hinge is expected to form at the ends of anchorage segments rather than at the beam-joint interface. As illustrated in Figure 2, the joint shear force can be reduced through balancing the input forces transferred from beam longitudinal reinforcements. Due to the opposite sign of bending moments at the beam-column interfaces across the joint core, the top reinforcements on one side and the bottom reinforcements on the other side are both under tension or compression. Hence, the forces taken by the horizontal segments of the proposed reinforcement detail can be balanced by the diagonal segments. To prevent the forces taken by the diagonal segments transferring to joint concrete, the diagonal segments are covered with PVC tubes.

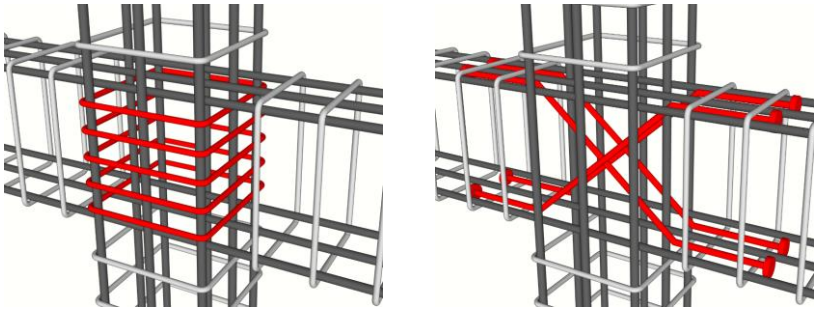

(a) conventional stirrups (b) proposed reinforcement detail

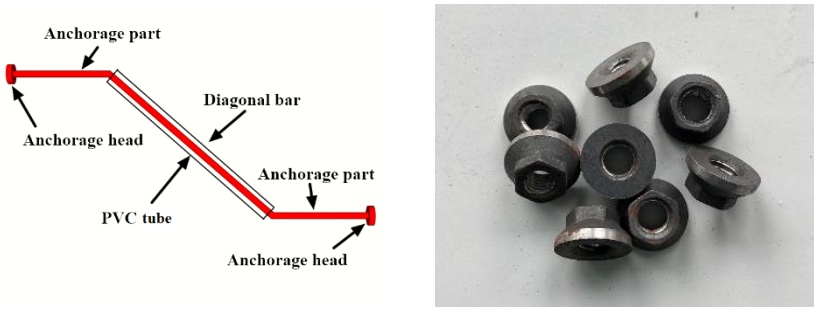

(c) single diagonal bar (d) steel anchorage heads

Figure 1. Schematic view of the reinforcement details for BCJs.

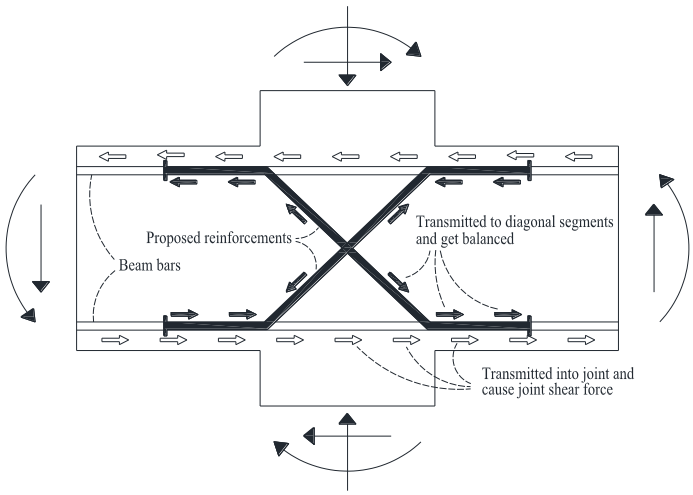

Figure 2. Input shear force reduction mechanism of the proposed reinforcement detail.

2.2 Specimen description

Four 2/3-scale RC interior BCJ specimens were designed and tested in this study. Except the horizontal stirrups in the joint cores, the specimens designed in accordance with GB50010 [4] have identical geometry and reinforcement details as shown Figure 3(a). The beam with a cross-section of 250 mm × 350 mm has an overall length of 2800 mm. Three D14 bars are placed symmetrically at top and bottom zones of beam sections as longitudinal reinforcements. The column with a square section of 300 mm × 300 mm has a total length of 2130 mm. Eight D16 bars are arranged evenly along the periphery as longitudinal reinforcements. D10 bars were adopted as the stirrups with a spacing of 100 mm for both beam and column. The thickness of concrete cover is 25 mm.

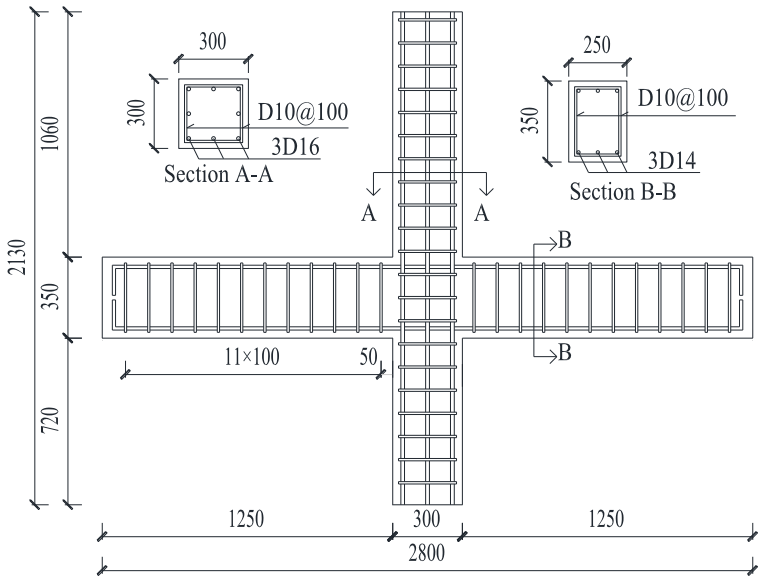

(a) Geometry and reinforcements of J1

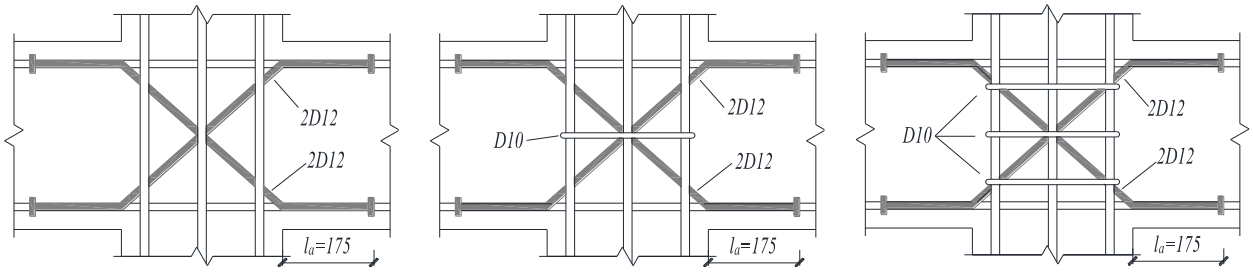

(b) Joint reinforcement of J2 (c) Joint reinforcement of J3 (d) Joint reinforcement of J4

Figure 3. Geometry and reinforcement details of specimens (Unit: mm).

The BCJ specimens were designed with different reinforcement details in the joint regions. Three layers of conventional stirrups at a spacing of 100 mm were adopted for specimen J1, while the proposed reinforcement detail is adopted for specimens J2-J4 as illustrated in Figures 3(b)-3(d). In specimen J2, conventional stirrups were completely replaced by two pairs of D12 diagonal bars with anchorages in the beams ends, while one and three D10 horizontal stirrups at a spacing of 100 mm were added to specimens J3 and J4, respectively. The anchorage length l_a of mechanically anchored deformed steel bars was determined based on Eq. (1) specified in GB50010 [4].

$$l_a=0.084f_yd/f_t \quad (1)$$

where f_y is the yield strength of steel bar, f_t is the tensile strength of concrete, and d is the diameter of steel bar. Based on the material properties measured, an anchorage length of 187 mm is obtained. It should be noted that Eq. (1) estimates the required anchorage length based on yielding of steel bars, while in this case the anchorage segments of the proposed reinforcement detail is not considered as yielded due to plastic hinge relocation. Consequently, the anchorage length is reduced to 175 mm, corresponding to half of the beam depth.

Material properties of steel bars and concrete were tested. Yield and ultimate strengths of deformed steel bars are given in Table 1. Ready-mix concrete was used to cast the four BCJ specimens. Cubic compressive strength f_{cu} based on 100 mm cubes at the 28th curing day was 43.8 MPa. The compressive

strengths of concrete on the day of testing for specimens J1-J4 were 43.6 MPa, 46.0 MPa, 45.6 MPa, and 46.5 MPa, respectively.

Table 1. Mechanical properties of steel bars.

Material properties	Steel bar			
	D10	D12	D14	D16
Yielding strength f_y (MPa)	450	453	443	460
Ultimate strength f_u (MPa)	635	645	668	650

2.3 Test setup and loading sequence

The test setup of BCJ specimens is shown in Figure 4. The bottom of the column was hinged to the strong floor through a fixture, while the top of the column was connected to a servo-hydraulic actuator for applying the horizontal load. A hydraulic jack was also installed at the top of the column to apply axial load through stressing four rods connecting the top plate with the bottom fixture. Both ends of beams were constrained in vertical direction only, thus they are free to rotate and move horizontally. With this test setup, the distances between contra-flexural points on beams and columns were 2400 mm and 2130 mm, respectively. Load cells were attached to the horizontal actuator and the column top to monitor horizontal reaction force and column axial force, respectively. A wire linear variable displacement transducer (LVDT) was used to record the induced column top displacement. Two rod LVDTs were installed on the back of joint core to monitor the shear deformation. In addition, strain gauges were installed on the beam longitudinal bars, the joint stirrups, and the proposed reinforcement detail to record their corresponding strain.

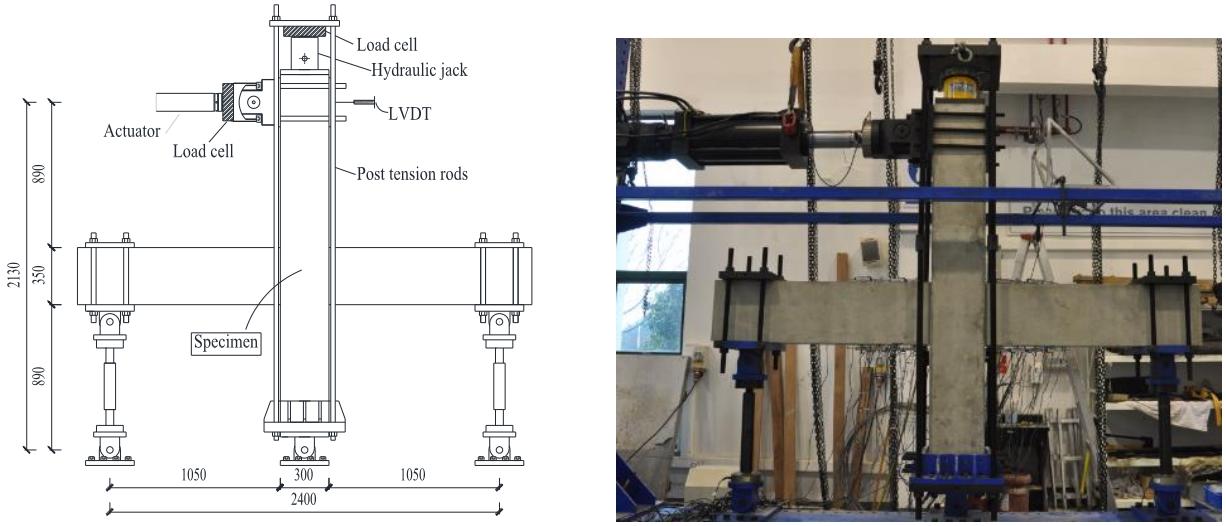

Figure 4. Test setup of BCJ specimens (Unit: mm).

The loading sequence for BCJs consists of two stages. At the first stage, a medium level [22–24] of column axial force of $0.2f_c'A_g$ was loaded, where f_c' is the cylinder compressive strength of concrete and A_g is the gross area of the column section. Here f_c' is taken as $0.8f_{cu}$ with f_{cu} being the cubic compressive strength of concrete on the day of testing. At the second stage, horizontal loading was applied at the column top following the displacement scheme illustrated in Figure 5. The displacement scheme was designed based on the control specimen (i.e. specimen J1), and then applied to the other

specimens. Prior to applying the horizontal load, the nominal flexural capacity M_{bu} of the beam section was calculated using the tested material properties and neglecting the partial safety factors. In the first cycle, the horizontal displacement was applied to the level when the bending moment reaches $0.75M_{bu}$ and the corresponding displacement was marked as $0.75\Delta_y$. The nominal yielding displacement Δ_y was subsequently calculated by linear extrapolation. In the following cycles, the displacement level was increased step by step to Δ_y, $2\Delta_y$, $3\Delta_y$, …, with each displacement level repeated twice. The specimens were loaded to failure when the applied force descended to 80% of the recorded peak load.

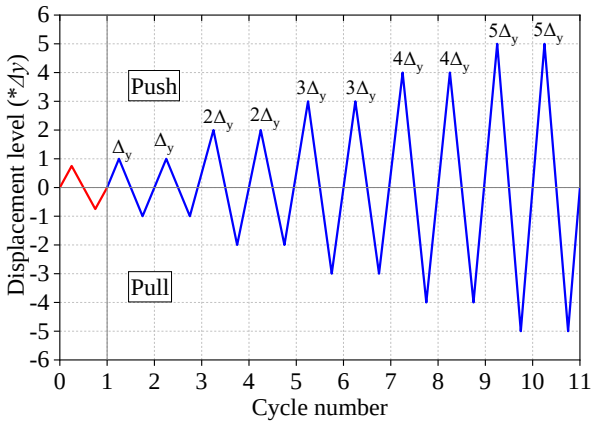

Figure 5. Loading history of applied horizontal displacement.

3. Test results and discussion

3.1 General observations and failure modes

Figure 6 shows the development of crack patterns at various positive displacements and failure modes of BCJ specimens. In specimen J1 with the conventional joint reinforcements, flexural cracks were first observed on the beams at the horizontal displacement of 11.3 mm. These flexural cracks evolved from top and bottom of the beams and propagated symmetrically towards the middle of the beam section. As the horizontal displacement increased to 15 mm, the first diagonal crack on the joint core was found. With further increase of displacement, the flexural cracks mainly developed at the beam-joint interfaces in width as these sections are subjected to higher bending moments. Meanwhile, the cracks at the joint core continuously propagated in terms of length and quantity. However, their width at the joint core was well restrained by the horizontal stirrups, which indicates the horizontal stirrups designed according to the code were able to resist the joint shear force. At the horizontal displacement of 75 mm, concrete spalling occurred at the beam-joint interfaces, followed by the formation of plastic hinges at the beam-column interfaces. There was more massive concrete spalling at the beam-joint interfaces as the displacement further increased, leading to the final failure of specimen J1. Generally, specimen J1 failed with the formation of plastic hinges at the beam-joint interfaces as shown in Figure 6(a).

Compared with specimen J1, the development of cracks on the beams of specimens J2-J4 was similar at the initial loading stage but different with further increased displacement. Flexural cracks first formed and propagated on the beams as the horizontal displacement increased. However, the development of flexural cracks mainly concentrated at the sections located at the ends of anchorage segments of the proposed reinforcement detail after the horizontal displacement reached 45 mm. These flexural cracks were much wider than those at other locations on the beams, as the anchorage segments

of the proposed reinforcement detail enhanced the flexural resistance of beam sections close to the joints. As the horizontal displacement further increased, several splitting cracks were observed near the ends of the proposed reinforcements, followed by concrete crushing and spalling. This indicates that the plastic hinges formed at the sections away from the beam-joint interfaces as shown in Figures 6(b)-6(d). Moreover, the plastic hinges in specimens J2-J4 spread in wider regions than those in specimen J1. With further cyclic loading, the spalling of concrete accompanied by the buckling of longitudinal bars occurred in the plastic hinge zones. Specimens J2-J4 eventually failed with the formation of plastic hinges at the ends of anchorage segments of the proposed reinforcement detail.

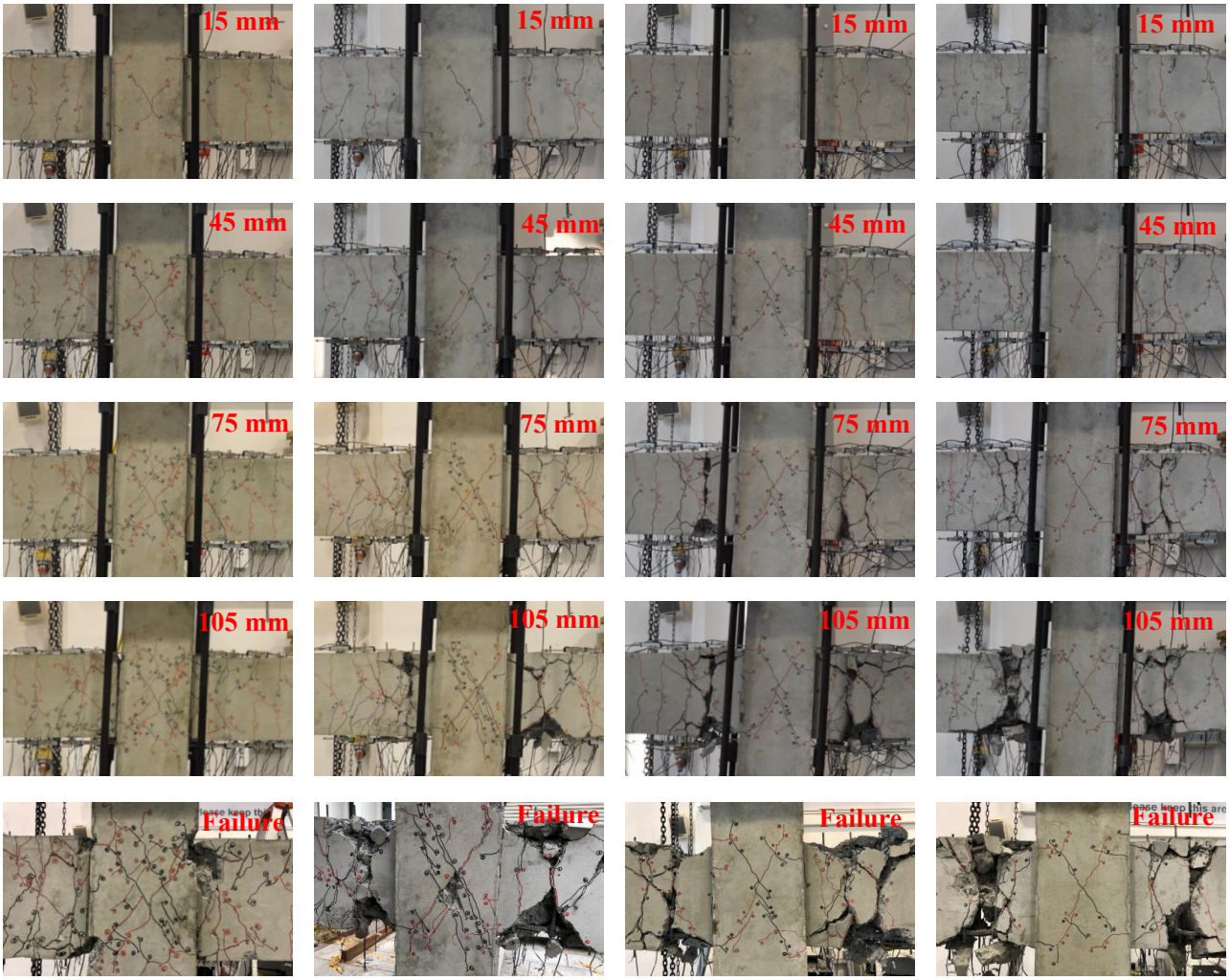

(a) J1 (b) J2 (c) J3 (d) J4

Figure 6. Development of cracks and failure modes of BCJ specimens.

The cracks within the joint cores in specimens J2-J4 with the proposed reinforcement detail mainly distributed along the diagonal directions, while those in specimen J1 with the conventional reinforcement distributed across the joint core. Moreover, specimens J2-J4 exhibited different levels of damage inside the joint cores, resulting from the combination of different quantities of stirrup with the proposed reinforcement detail. Diagonal cracks were initially observed in the joint cores at the horizontal displacement of 15 mm for the specimens. As there was no stirrup in the joint core of specimen J2, the joint core was less restrained against the development of cracks. Consequently, the

cracks propagated quickly along the diagonal directions in terms of both width and quantity, followed by concrete spalling inside the joint core due to the repeated opening and closing of the cracks as shown in Figure 6(b). With the addition of one layer of stirrup in specimen J3, the cracks inside the joint core were properly controlled in terms of width and quantity. There were limited number of hairline diagonal cracks in the joint core as shown in Figure 6(c). It indicates that adding one layer of stirrup is able to activate the truss mechanism to sustain the stresses developed inside the joint core. For specimen J4 with three layers of stirrups inside the joint core, there was a limited improvement in cracking behaviour as compared with specimen J3. Adding more stirrups in the joint core only slightly decreased the number of cracks as seen in Figure 6(d). It should be noticed that the stirrups in specimen J4 are placed with a relatively small spacing due to the limited height of the beams, which causes similar cracking behaviour for specimens J3 and J4. In summary, joint stirrup is necessary to control the cracks inside the joint core for BCJs with the proposed reinforcement detail. However, the amount of joint stirrups can be reduced from three layers to one layer in specimen J3 as more stirrups in specimen J4 result in a marginal effect on further reducing the cracks inside the joint core.

3.2 Hysteretic behaviour

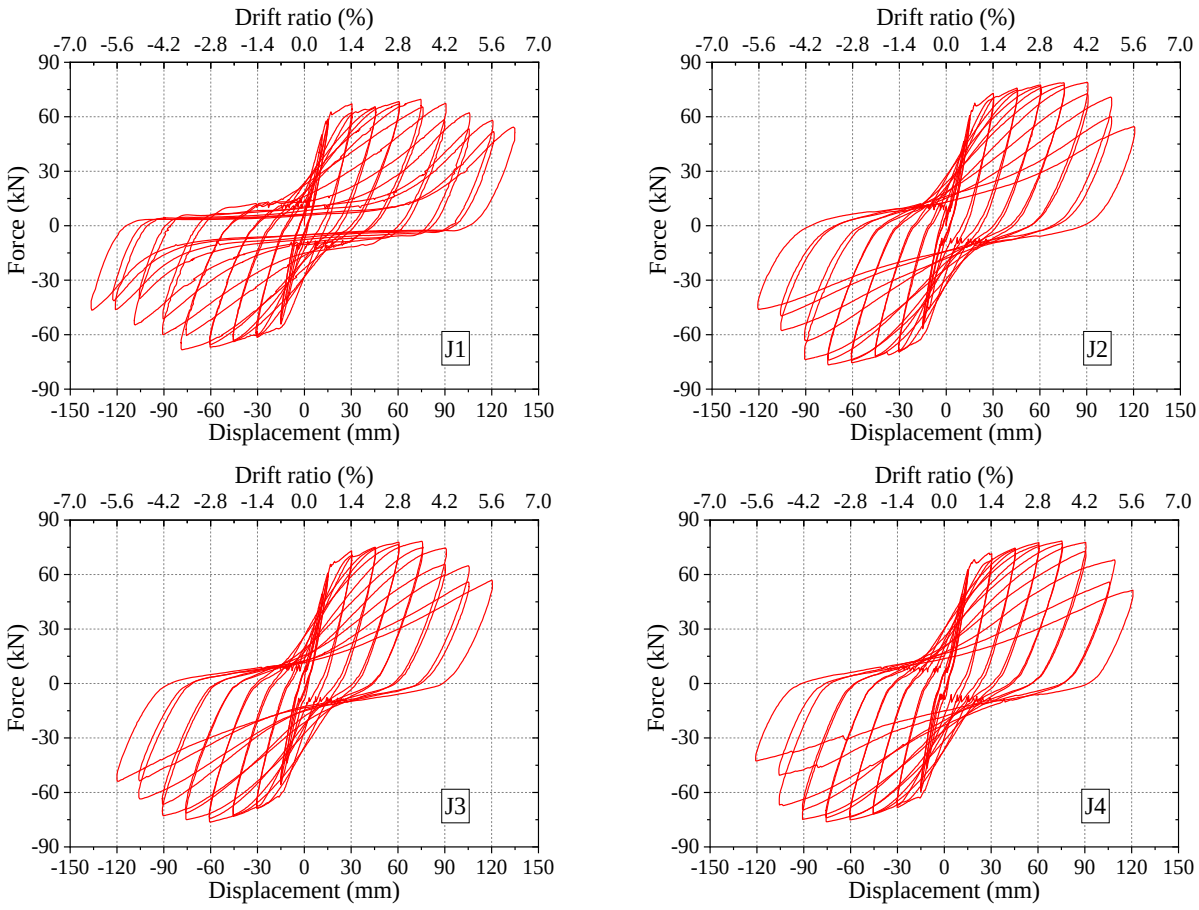

Figure 7. Load-displacement relationship of BCJ specimens.

Figure 7 shows the hysteretic relationships of horizontal force and displacement at the column tip for BCJ specimens. In general, the horizontal force is linear to the displacement for all specimens at the initial loading stage, indicating that the deformations of BCJs are mainly within elastic range. After entering the yielding stage, the hysteretic loops of specimens become plumper. The nonlinear

deformation of specimens occurs due to the yielding of steel reinforcement and the cracking of concrete. With the increasing horizontal displacement, their loading and unloading stiffness decreases and the area of each hysteretic loop becomes larger. At the late loading stage, the hysteretic loops of BCJs with the conventional stirrups and the proposed reinforcement detail have different shapes. There is a smooth sliding stage during the unloading and reloading stages in specimen J1. This means that the horizontal force keeps almost constant under various horizontal displacements, resulting from severe bonding failure between beam longitudinal bars and joint concrete. Consequently, the beam longitudinal bars slipped against joint concrete until the opened cracks at the beam-joint interfaces closed. Although specimen J1 could sustain the load after sliding, the slippage of beam longitudinal bars inside the joint core leads to a significant pinching phenomenon in the hysteretic loops. This is consistent with the findings of a previous study by Alaee and Li [25]. Compared to specimen J1, the sliding phenomenon is well prevented for specimens J2-J4, indicating that the bonding between beam longitudinal bars and concrete inside the joint core is well maintained. Consequently, the hysteretic loops for specimens J2-J4 are plumper than that for specimen J1, especially at the late stage of loading. For the specimens with the proposed reinforcement detail, the addition of stirrups has a negligible impact on their hysteretic behaviour, as the overall behaviour of specimens is controlled by the plastic hinges formed in beams.

3.3 Envelope curves and displacement ductility

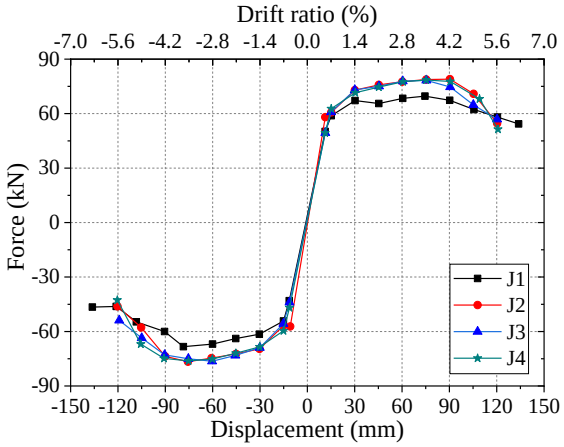

Figure 8. Envelope curves of hysteretic loops for specimens.

Figure 8 shows the envelope curves of hysteretic loops for the BCJ specimens. The four BCJ specimens exhibit similar force-displacement relationships at the initial stage of loading as they are mainly within the elastic stage. Afterwards, specimen J1 gradually enters the yielding stage, followed with a reduction of horizontal force after the formation of plastic hinges. Specimens J2-J4 with the proposed reinforcement detail sustain higher loads than specimen J1 under the same displacement level. With further increased displacement after the peak loads, the loads of specimens J2-J4 drop faster than that of specimen J1, which is mainly related to the buckling of beam longitudinal bars due to the more severe concrete spalling in specimens J2-J4. At the final stage of loading, the loads of specimens J2-J4 are even lower than that sustained by specimen J1. The loading capacities of the specimens at the push and pull loading directions are given in Table 2. Compared to the specimen J1 with conventional stirrups, the loading capacities of specimens J2-J4 with the proposed reinforcement detail are increased by 11.6% to 13.4%. For the three specimens with the proposed reinforcement, the envelope curves are

comparable as they are dominated by the yielding of the beams with the same reinforcements.

The displacement ductility μ defined as the ratio of ultimate displacement Δ_u to yielding displacement Δ_y is calculated for specimens at the push and pull loading directions. The ultimate displacement is defined as the post-peak displacement at 80% of the peak load, while the yielding displacement is determined by the energy balance method [26]. Table 2 shows the calculation of yielding displacement, ultimate displacement and ductility of specimens. The specimen J1 achieves a displacement ductility of 6.8 and 4.9 in the push and pull directions, respectively. With the proposed reinforcement detail, the displacement ductility of specimens J2-J4 is slightly decreased, which agrees with the faster drop of forces in the envelope curves. This reduction of ductility is mainly associated to the buckling of beam longitudinal bars and the spalling of concrete in the plastic hinge zones. Ductility of specimens J3 and J4 is marginally higher than that of specimen J2. It indicates that addition of stirrups inside the joint core has a limited improvement on the ductility of BCJs with the proposed reinforcement detail. As specimens J2-J4 finally failed with the formation of beam plastic hinges, adding more stirrups inside joint core has a negligible impact on the overall displacement ductility of BCJs.

Table 2: Concrete strength, loading capacity and displacement ductility of specimens.

Specimen	Push direction				Pull direction			
	F_u (kN)	Δ_y (mm)	Δ_u (mm)	μ	F_u (kN)	Δ_y (mm)	Δ_u (mm)	μ
J1	69.6	19.0	129.1	6.8	68.3	22.3	108.4	4.9
J2	78.9 (13.4%)	21.9	112.4	5.1	76.6 (12.2%)	23.6	101.9	4.3
J3	78.3 (12.5%)	20.3	109.3	5.4	76.4 (11.9%)	21.9	108.6	5.3
J4	78.5 (12.8%)	21.4	112.8	5.3	76.2 (11.6%)	22.1	109.2	4.9

Note: the number in parentheses indicates the improvement compared to the control specimen.

3.4 Energy dissipation

Figure 9 shows the cumulative energy dissipation of BCJ specimens against the horizontal displacement. The cumulative energy dissipation is calculated by summing up the areas of previously accomplished hysteretic loops. Generally, the cumulative energy dissipation of BCJ specimens increases with the horizontal displacement. Before the horizontal displacement reaches 30 mm, those specimens dissipate similar energy regardless of the joint reinforcements. Afterwards, specimens J2-J4 with the proposed reinforcement detail dissipate higher cumulative energies than the control specimen. This is mainly attributed to the higher force sustained by the specimens and the better bonding between beam longitudinal bars and concrete within the joint cores. Among those specimens with the proposed reinforcement detail, specimens J2 and J3 show similar energy dissipation capacity, which indicates that the addition of one stirrup has a limited effect on improving the energy dissipation. Nevertheless, further increasing the amount of stirrups to three layers leads to the highest energy dissipation in specimen J4. This means that the addition of three layers of stirrups to the proposed reinforcement detail is beneficial in improving the energy dissipation of BCJs. As compared with specimen J1, the cumulative energy dissipation of specimens J2, J3 and J4 is increased by 10.6%, 7.3% and 19.2%, respectively.

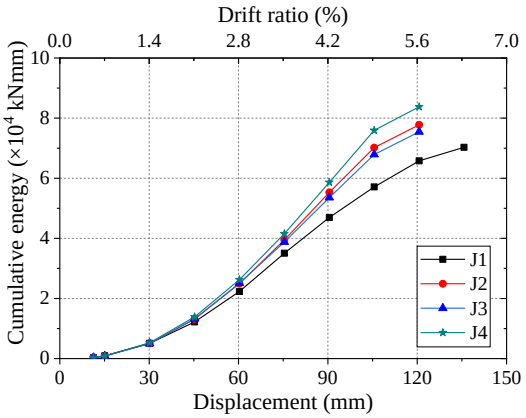

Figure 9. Cumulative energy dissipation of specimens at various displacements.

3.5 Stiffness degradation

Figure 10 shows the stiffness degradation of BCJ specimens at various displacements. Secant stiffness defined as the slope of the line connecting the peak loads at the positive and negative directions is calculated, based on the first cycle at each displacement level. Generally, the stiffness of the BCJ specimens decreases as the displacement increases. The specimens have similar stiffness at the initial stage of loading. As the displacement increases, the stiffness of specimen J1 drops slightly faster than that of the other specimens. This reflects that the proposed reinforcement detail has a negligible influence on the initial stiffness of BCJs, but could slightly delay the degradation of stiffness. However, the degradation rates of stiffness tend to be identical for specimens J1-J4 at the advanced stage of loading. The stiffness degradation curves of specimens J2-J4 are almost overlapped, indicating that the variation of joint stirrups could not change the stiffness of specimens. Overall, the adoption of the proposed joint reinforcement detail and the amount of stirrups have a marginal impact on the stiffness degradation of BCJs.

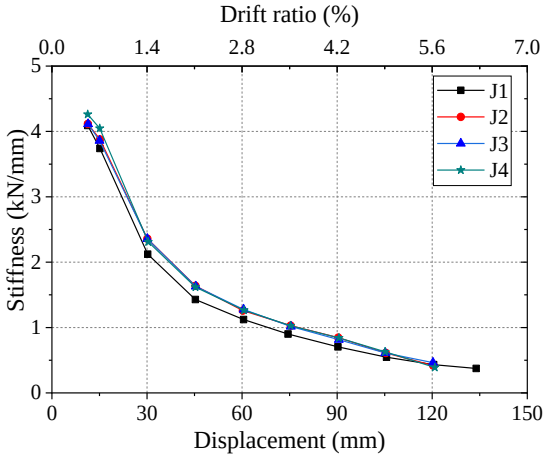

Figure 10. Secant stiffness of specimens at various displacements.

3.6 Joint distortion

Figure 11 shows the calculation of joint distortion and the relationship of joint distortion to displacement for the tested specimens. Here, the joint distortion is calculated based on the measurements of a pair of LVDTs installed diagonally in the joint core as shown in Figure 11. At the

initial stage of loading, the joint distortion for all the specimens gradually increases with the horizontal displacement, resulting from the increasing joint shear force. For specimen J1, the joint distortion tends to be stable and even slightly decreases after the horizontal displacement reaches 75 mm, as the deformation of specimen J1 mainly focuses on the plastic hinges developed at beam-joint interfaces at the late stage of loading. However, joint distortion of specimen J2 without conventional stirrup increases considerably after reaching the horizontal displacement of 75 mm. For instance, specimen J2 exhibits 5 times higher joint distortion that specimen J1 at the horizontal displacement of 120 mm. This highlights the importance of joint stirrup in controlling the joint distortion and agrees with the observed failure mode of specimen J2. Combining one layer of stirrup with the proposed reinforcement detail in specimen J3 results in a significant reduction of joint distortion. The joint distortion of specimen J3 is lower than that of specimens J1 and J2. As compared with specimen J2, the adding one layer of stirrup reduces joint distortion by around 90% in specimen J3 at the displacement of 120 mm. Adding two layers of stirrups can further reduce the joint distortion in specimen J4. For example, the joint distortion of specimen J4 is almost half of that of specimen J3 after reaching the displacement of 60 mm. Nevertheless, additional two layers of stirrups in specimen J4 is not as effective as the one layer of stirrup in specimen J3. Moreover, the joint distortions of both specimen J3 and J4 are lower that specimen J1 with the conventional stirrups. This indicates that the existence of joint stirrup is crucial in controlling the joint distortion, but further addition of stirrups have a marginal impact on restraining the distortion of joint cores in BCJs.

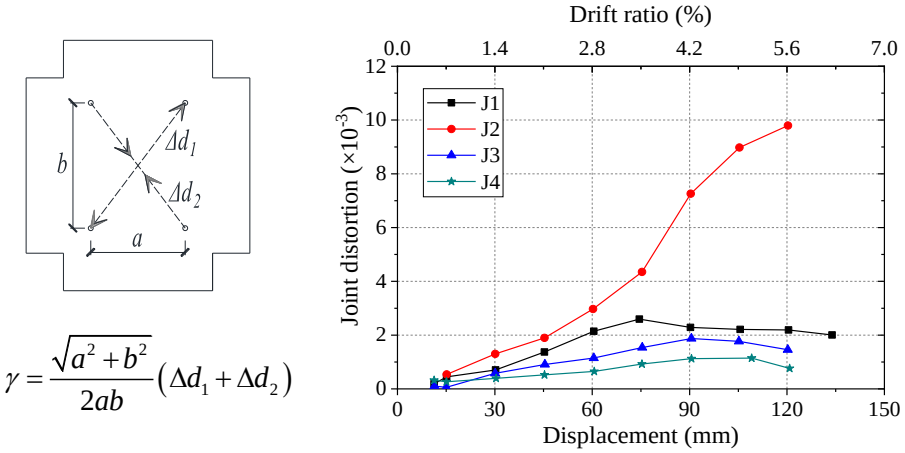

Figure 11. Computation and results of joint distortion at various displacements.

3.7 Strain of beam longitudinal bars

Figure 12 presents the strain profiles of the upper beam longitudinal bars at different displacement levels. The horizontal and vertical axes indicate the relative distances to the joint centre and the strains of bars, respectively. Only strains of beam bars before the displacement of 45 mm are shown in the figures, due to the malfunction of strain gauges under the repeated loadings. At the displacement of 30 mm, the strains of bars in all specimens are generally subjected to tension and compression in the left and right beams, respectively. The strains of beam bars in specimen J1 increase gradually as they get closer to the beam-column interfaces. The strains of beam bars at the left beam-joint interface reach the yielding level at the displacement of 15 mm. At the displacement of 45 mm, the beam bars at both left and right column faces are subjected to a high tensile strain. It indicates that there is a significant

bonding deterioration between beam bars and concrete inside the joint core for specimen J1. For specimens J2-J4 with the proposed reinforcement detail, the strains of beam bars distribute more uniformly, and their highest strains occur at a section away from the beam-joint interfaces. This is mainly caused by the enhanced flexural resistance at the beam ends with the incorporation of anchorage segments of the proposed reinforcement detail. Besides, the beam bars in specimens J2-J4 enter the yielding stage after reaching the displacement of 30 mm, which is delayed when compared to that in specimen J1. Moreover, the slopes of strain distribution in the joint regions of specimens J2-J4 are lower than that of specimen J1. It indicates that the forces inputted into the joint cores through bonding are reduced for the specimens with the proposed reinforcement detail. The specimens with different layers of stirrups show similar strain profile for the beam bars. Increasing the layers of stirrups inside the joint cores has a limited influence on the strain distribution of beam bars in the joint regions.

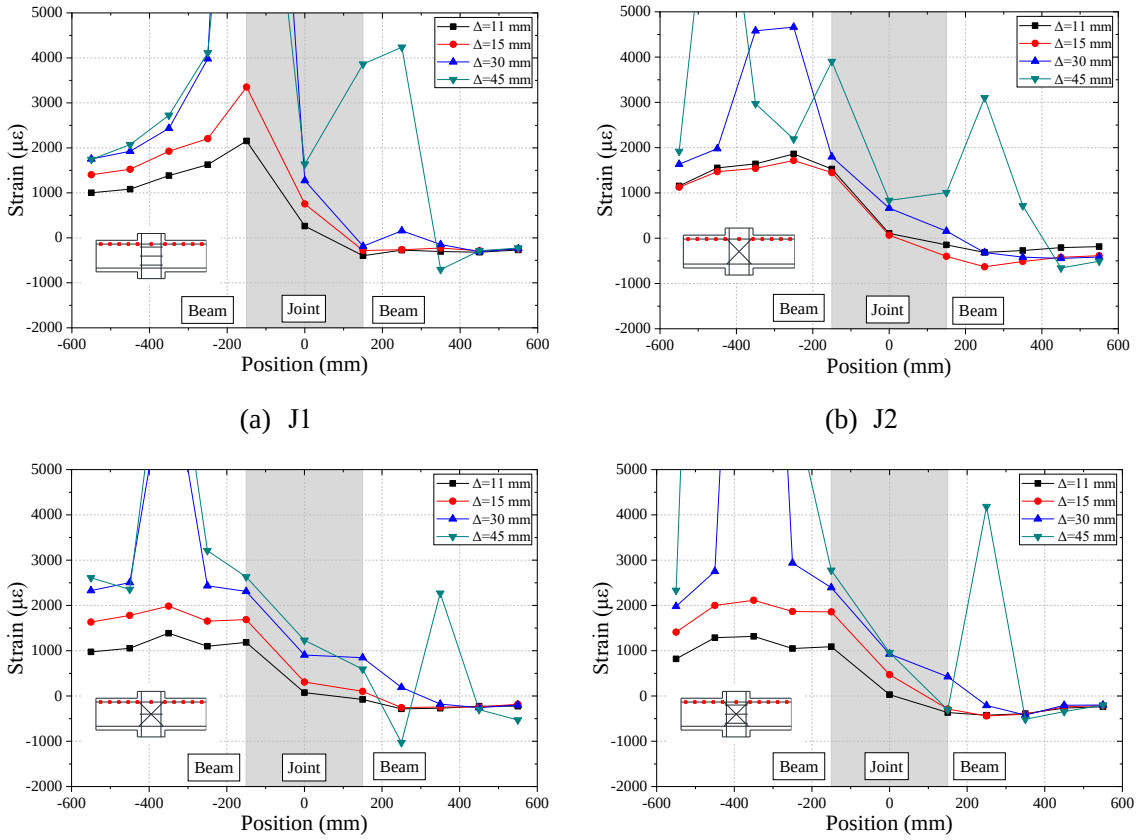

(a) J1 (b) J2

(c) J3 (d) J4

Figure 12. Strain profiles of the upper beam longitudinal bars under pushing action.

3.8 Strain of joint stirrup

Figure 13 shows the strain of joint stirrups at various displacements for BCJ specimens. Here, specimen J2 is not included as there is no stirrup in its joint core. Generally, the strains of stirrups in specimens J1, J3 and J4 first increase with the horizontal displacement, followed with a reduction as the horizontal displacement further increases. The initial increase of strain of joint stirrups is mainly caused by the enhanced involvement in shear resistance through the truss mechanism. After reaching peak strains, the strains of joint stirrups in all specimens drop with the increased displacement. On one hand, bond deterioration between the beam longitudinal bars and joint concrete under cyclic loading

reduces the shear resistance contributed by the truss mechanism. On the other hand, the forces on the specimens drop after reaching their loading capacities as seen in the envelope curves of hysteretic loops. Moreover, the damage of BCJ specimens concentrated on beams instead of joint cores in specimens J1, J3 and J4 at the late stage of loading.

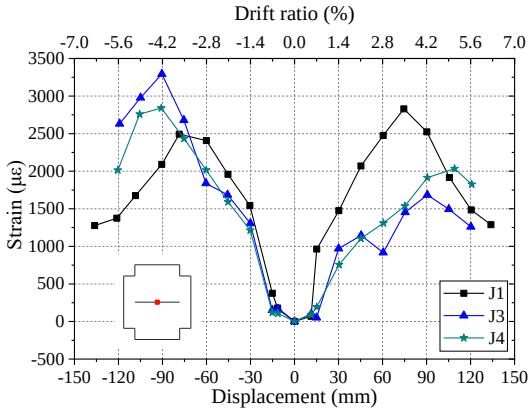

Figure 13. Strain of joint stirrups at various displacements.

The strain of joint stirrup in specimen J1 is clearly higher than that in specimens J3 and J4 at the early stage of loading. It indicates that force transmitted into the joint core of specimen J1 is larger than that of the other two specimens. Besides, the strain of joint stirrup in specimen J1 starts to drop at the displacement of 75 mm, while strains of joint stirrups in specimens J3 and J4 drop at the displacement of 90 mm. This indicates that the contribution of truss mechanism within the joint cores in specimens J3 and J4 deteriorates at the later stage of loading. Essentially, the plastic hinge relocation in specimens J3 and J4 improves the bonding condition between beam longitudinal bars and joint concrete, which delays the deterioration. Specimens J3 and J4 with different layers of stirrups exhibit similar strain of stirrups, indicating the quantity of stirrups inside the joint cores marginally affects their strains for BCJs with the proposed reinforcement detail.

3.9 Strain of the proposed reinforcements

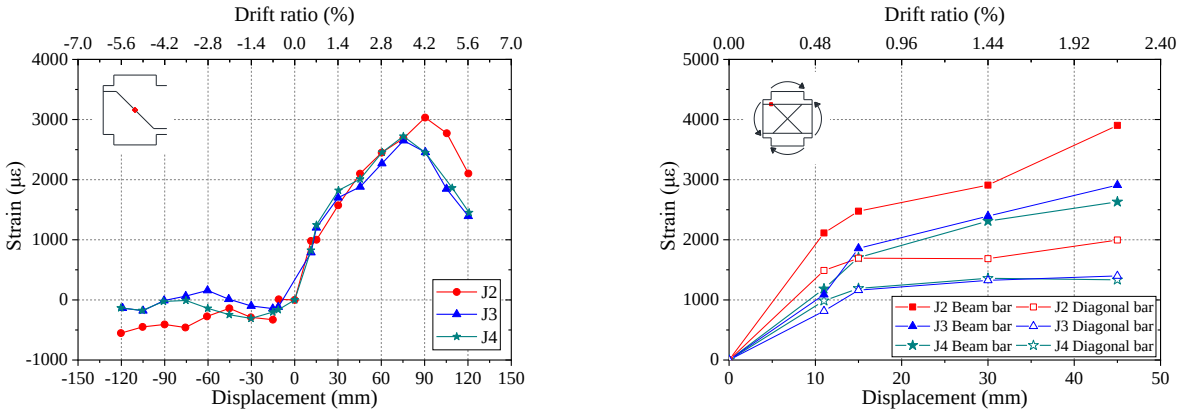

(a) at diagonal part (b) at beam-joint interface

Figure 14. Strain of the proposed reinforcements at various displacements.

Figure 14(a) shows the strain on diagonal segments of the proposed reinforcement detail for specimens J2-J4. The diagonal bars inside the joint cores are under tension and compression when BCJ specimens are loaded in push and pull directions, respectively. Generally, the strain of diagonal bars is more significant in tension than in compression. Under the push loading, the strain of diagonal segments ascends as the horizontal displacement increases up to 90 mm, followed with a reduction as the horizontal displacement further increases. This reduction could result from two reasons: Firstly, the force of BCJ specimen decreases at the late stage of loading as discussed previously for the envelope curves of the hysteretic loops. Secondly, the deformation in BCJs was shifted from the joint cores to the plastic hinge zones at beam ends at the advanced stage of loading. Moreover, the maximum strain of diagonal bars in specimen J2 is slightly higher than that of specimens J3 and J4, as specimen J2 experienced a higher joint distortion. Specimens J3 and J4 have similar strain for diagonal bars inside the joint cores. It indicates that increasing amount of stirrups have a marginal impact on the forces taken by the diagonal bars.

Figure 14(b) shows the strain of steel bars at the beam-joint interface for specimens J2-J4 under the push loading. Both beam longitudinal bars and anchorage segments of the proposed reinforcement detail are included. The beam longitudinal bars experienced a higher strain than the anchorage segments of the proposed reinforcement, due to the better anchorage condition of beam longitudinal bars. It can be seen that beam longitudinal bars of specimen J2-J4 typically undergo double strain than the anchorage segments of diagonal bars. The strain of bars at the beam-joint interface in specimen J2 is higher than that in specimens J3 and J4, indicating that the addition of joint stirrups helps control the integrity of joint regions and reduces the input shear force inside the joint cores. However, specimens J3 and J4 show similar strains for beam longitudinal bars and anchorage segments of diagonal bars. It indicates that increasing the amount of stirrup has very limited effect on reducing the strain of beam longitudinal bars at the beam-joint interfaces.

4. Analytical study

4.1 Model description

Figure 15 illustrates the mechanism of plastic hinge relocation for a BCJ with the proposed reinforcement detail. The upper graph shows the applied bending moment (shaded) and the flexural capacity (void) along the beam. With the anchorage segments of the proposed reinforcement detail, the flexural capacity of beam ends is increased from M_{bu} to M_{bu}'. To relocate plastic hinges from the beam-column interfaces to the ends of anchorage segments, the applied bending moment M_b at the ends of anchorage segments shall be equal to M_{bu}. Therefore, the applied bending moment at the beam-joint interfaces M_b' can be calculated by extrapolation based on Eq. (2).

$$M_b' = M_{bu} l_b / (l_b - l_a) \tag{2}$$

where l_b is the distance from the beam contra-flexure point to the beam-joint interface, and l_a is the anchorage length of diagonal bars. To achieve the plastic hinge relocation, the flexural capacity of beam section at the beam-joint interfaces M_{bu}' should be higher than the applied bending moment, as given in Eq. (3).

$$M_{bu}' > M_b' \tag{3}$$

Therefore, a proper anchorage length l_a of diagonal bars needs to be determined for achieving the

plastic hinge relocation. If the anchorage length is too small, the plastic hinge relocation may not be evident as the forces taken by the anchorage segments are insufficient. Moreover, relocating plastic hinge by a short distance may still result in the yielding penetration of beam longitudinal bars into the joint core, leading to a higher joint shear force. If the anchorage length of diagonal bars is too long, the applied bending moment at the beam-joint interfaces may exceed the flexural capacity of beam. The plastic hinges consequently form at the beam-joint interfaces, leading to the failure of the joint cores. Therefore, the plastic hinge relocation occurs only when the anchorage length of diagonal bars is within a proper range. In this study, specimens J2, J3 and J4 were designed with a proper anchorage length for the diagonal bars.

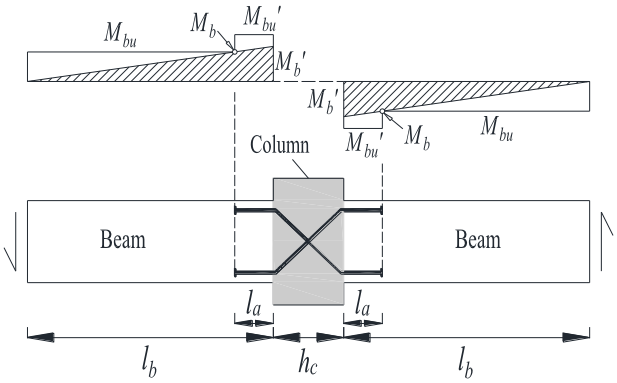

Figure 15. Design of plastic hinge relocation.

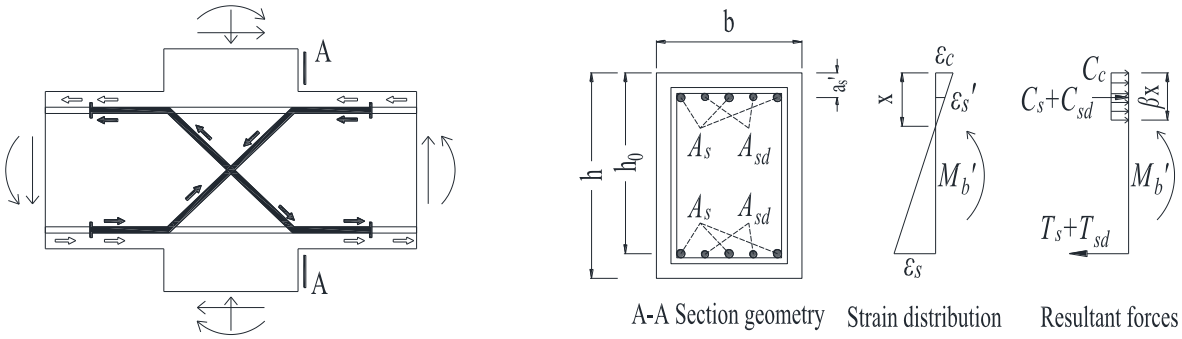

(a) Force flow on steel bars. (b) Sectional analysis of A-A section.

Figure 16. Illustration of input shear force reduction.

Figure 16 shows the input shear force reduction mechanism of the proposed reinforcement detail in BCJs. The force flow on the beam longitudinal bars (void) and the proposed reinforcement detail (solid) are plotted in Figure 16(a). At the beam-joint interfaces, both beam longitudinal bars and anchorage segments of the proposed detail contribute to the flexural resistance of beam section. The forces on the beam longitudinal bars are transmitted into the joint core through bonding, causing shear force inside the joint core. The forces on the anchorage segments of the proposed detail are transmitted into diagonal segments and self-balanced inside the joint core. To quantify the input joint shear force, section analysis at the beam-joint interface (e.g. A-A section) is performed as shown in Figure 16(b). Plane strain distribution is assumed, ε_s and ε_s' are the tensile and compressive strains of beam longitudinal bars, respectively. ε_c is the compressive strain of concrete at the top surface. The total forces of reinforcements and concrete can be calculated based on their material constitutive laws. Here

the resultant compressive force of concrete is determined based on Eq. (4) in accordance with the code GB50010 [4]. Uniaxial behavior of steel bars is assumed to be elastic-perfectly-plastic, therefore, the tensile and compressive forces of beam longitudinal bars are calculated by Eqs. (5) and (6), respectively.

$$C_c=\alpha_1 f_c \beta_1 x b \tag{4}$$

$$T_s=\varepsilon_s E_s \tag{5}$$

$$C_s=\varepsilon_s' E_s \tag{6}$$

where α_1 and β_1 are the parameters depending on ε_c, x is the height of concrete compression zone, and E_s is the elastic modulus of steel bars. The strain on the anchorage segments of the proposed reinforcement detail is taken as half of that on the beam longitudinal bars, as discussed in Section 3.9. Consequently, $T_{sd}=0.5\varepsilon_s E_s$ and $C_{sd}=0.5\varepsilon_s' E_s$ are the tensile and compressive forces on the anchorage segments of the proposed reinforcement detail. The above variables can be determined based on the equilibrium conditions in Eqs. (7) and (8).

$$C_c+C_s+C_{sd} = T_s+T_{sd} \tag{7}$$

$$C_c(h_0-0.5\beta x)+(C_s+C_{sd})(h_0-a_s')=M_b' \tag{8}$$

The input joint shear force V_j can be consequently determined based on force equilibrium in the joint core as shown in Figure 17. Only the forces on beam longitudinal bars and concrete are included, as the forces on the proposed reinforcement detail are self-balanced through the diagonal bars. T_{s1}, T_{s2}, T_{s3} and T_{s4} are the tensile forces on beam and column longitudinal bars, while C_{s1}, C_{s2}, C_{s3} and C_{s4} are the compressive forces on beam and column longitudinal bars. C_{c1}, C_{c2}, C_{c3} and C_{c4} are the compressive forces on concrete. V_b and V_c are the shear forces on beam and column, respectively. Thus, the input shear force V_j can be computed as in Eq. (9).

$$V_j=C_s+C_{c1}+T_{s2}-V_c \tag{9}$$

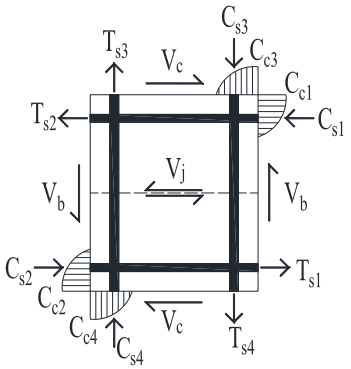

Figure 17. Forces acting on an interior BCJ.

To estimate the joint shear capacity V_{ju}, Eqs. (10)-(12) specified in the code GB50010 [4] are adopted. The equations consider the shear resistance of joint contributed from concrete, joint reinforcements, and the effect of column axial load, while limiting an upper bound to avoid concrete crushing.

$$V_{ju}=min(V_{ju1}, V_{ju2}) \tag{10}$$

$$V_{ju1}=0.353f_c'b_jh_j \quad (11)$$

$$V_{ju2}=(1.1f_yb_jh_j+0.05N+f_{yv}A_{svj})/0.85 \quad (12)$$

where f_c' and f_t are the compressive and tensile strength of concrete, respectively. b_j and h_j are the width and height of joint, respectively. N is the column axial force. f_{yv} and A_{svj} are the yielding strength of joint stirrups and total sectional area of joint stirrups, respectively. Based on the above analysis, the failure mode can be predicted, and loading capacity F_u of BCJs can be subsequently calculated based on force equilibrium. Figure 18 shows the procedure for predicting the failure mode and loading capacity of BCJs.

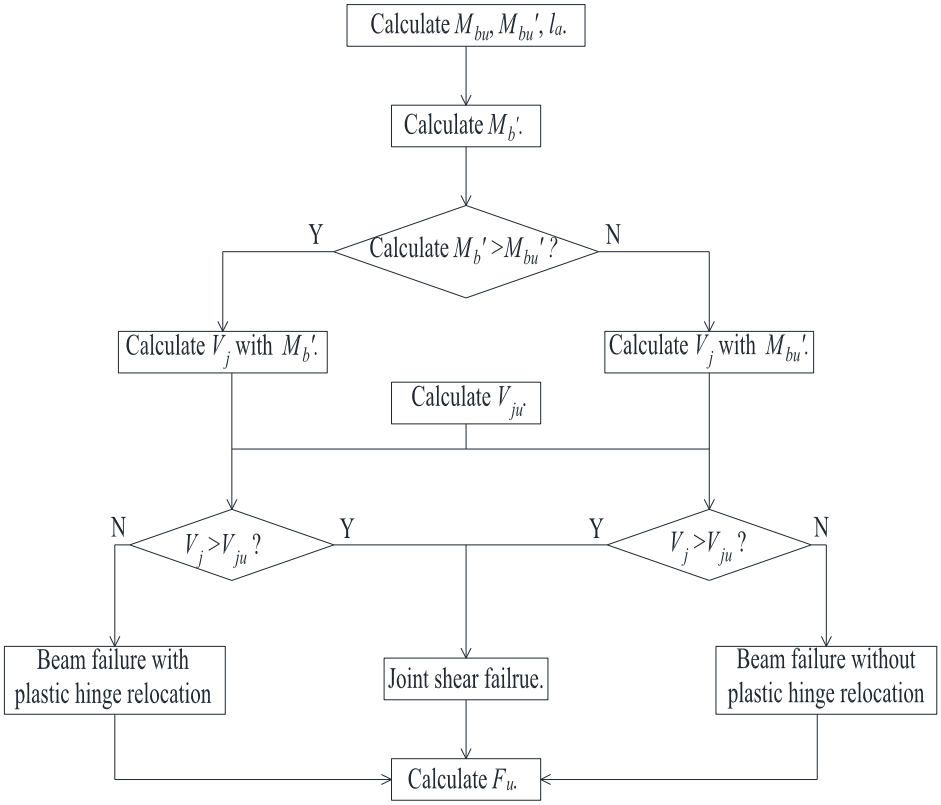

Figure 18. Procedure for predicting failure modes and loading capacity of BCJs.

4.2 Comparison between analytical and experimental results

Comparison of results from analytical model and experimental tests for the four specimens is shown in Table 3. It is worth noting that an over-strengthening factor of 1.25 for beam longitudinal bars was adopted to calculate joint shear force V_j for specimen J1, as the yielding of beam longitudinal bars was assumed at the beam-joint interfaces. Specimens J2-J4 satisfy the requirement specified in Eq. (3) for achieving beam plastic hinge relocation, which agrees with the observed failure modes in the test. It indicates that the developed analytical model is able to accurately predict the occurrence of plastic hinge relocation for BCJs with the proposed reinforcement detail. For specimens J1, J3 and J4, the predicted joint shear forces V_j is lower than joint shear capacities V_{ju}, indicating that these joint cores have enough strength to resist the input shear force. Furthermore, the loading capacities of BCJs were properly predicted as the ratio of tested to predicted loading capacity of BCJs ranges from 0.99 to 1.19, especially for specimens J1, J3 and J4 whose failure modes are correctly predicted. Nevertheless, the predicted joint shear force of specimen J2 is higher than its shear capacity, which results in a joint

shear failure in the prediction. This is different from the observed failure occurred at both beams and joint, resulting from underestimation of joint shear capacity based on Eqs. (10)-(12) specified in the code. Overall, the developed analytical model is able to accurately predict the failure mode and loading capacity of BCJs with the proposed reinforcement detail.

Table 3. Comparison of analytical and test results.

Spec.	M_{bu} (kNm)	M_b' (kNm)	M_{bu}' (kNm)	V_j (kN)	V_{ju} (kN)	Prediction		Test		$F_{u.t}/F_{u.p}$
						Failure mode	$F_{u.p}$ (kN)	Failure mode	$F_{u.t}$ (kN)	
J1	61.4	N/A	N/A	394.6	599.3	B	65.9	B	69.6	1.06
J2	61.7	73.2	89.8	385.9	313.1	J	66.3	J+B	78.9	1.19
J3	61.7	73.1	89.3	381.8	394.8	B	78.5	B	78.3	0.99
J4	61.8	73.3	90.4	386.4	564.1	B	78.6	B	78.5	0.99

Note: B - beam failure, J - joint failure.

5. Conclusions

This paper investigated the effectiveness of using unbonded diagonal bars with horizontal anchorage segments along beams to replace conventional stirrups for RC interior BCJs. Four BCJ specimens, including one control specimen designed in accordance with current code and three specimens adopting the proposed reinforcement detail, were prepared and tested under quasi-static cyclic loading. Seismic performances of the BCJ specimens were compared in terms of failure mode, hysteretic behaviour, energy dissipation, stiffness degradation, joint distortion and strain of reinforcements. An analytical model was also proposed to predict the failure mode and loading capacity of BCJs with the proposed reinforcement detail. Based on the test results and discussion, the following conclusions can be drawn:

(1) The proposed reinforcement detail for BCJs is able to move the plastic hinges away from the beam-joint interfaces as its anchorage segments enhance flexural capacities of beam sections close to the joint. The combined use of conventional stirrup and the proposed reinforcement detail significantly reduces the tendency of cracking inside the joint core.

(2) The adoption of the proposed reinforcement detail increases the loading capacity of BCJs by 13.4% as compared to BCJ with the conventional stirrups. This is achieved as the length of the force arm is reduced after the relocation of the plastic hinge. The proposed reinforcement detail for BCJs also enhances the energy dissipation, stiffness and ameliorates joint distortion, although the displacement ductility is slightly reduced. Further increasing the amount of joint stirrups has a marginal impact on the performance of BCJs with the proposed reinforcement detail.

(3) The BCJs with the proposed reinforcement detail possess the improved bonding between longitudinal bars and concrete inside the joint core. This is achieved through reducing the shear force transmitted into the joint core under the reduced yielding penetration and force self-balance mechanism. The strain on the anchorage segments of the proposed reinforcement detail is around half of that on beam longitudinal bars at the beam-joint interface.

(4) The developed analytical model can adequately predict the failure mode and the loading capacity of BCJs with the proposed reinforcement detail. The loading capacity is underestimated for the BCJ failed in joint shear, as the joint shear strength is estimated based on the code. However, the model can still be applied for conservative design purpose.

(5) Replacing horizontal stirrups with the proposed reinforcement detail in BCJs can alleviate the reinforcement congestion inside the joint core. However, conventional stirrups are still necessary to confine the joint cores and resist shear forces in BCJs with the proposed reinforcement detail.

Acknowledgement

The authors wish to acknowledge the financial support of National Natural Science Foundation of China (Grant No. 51708306), Zhejiang Provincial Natural Science Foundation of China (Grant No.: LGF19E080008) and Ningbo Municipal Bureau of Science and Technology (Grant No.: 2019B10048). Special thanks are also extended to the support of specimen preparation from the Ningbo Preca Construction Technology Co., Ltd.

References

[1] Chetchotisak P, Arjsri E, Teerawong J. Strut-and-tie model for shear strength prediction of RC exterior beam–column joints under seismic loading. Bull Earthq Eng 2020;18:1525–46.
[2] Pauley T, Priestley MJN. Seismic Design of Reinforced Concrete and Masonry Buildings. 1992.
[3] Tapan M, Comert M, Demir C, Sayan Y, Orakcal K, Ilki A. Failures of structures during the October 23, 2011 Tabanlı (Van) and November 9, 2011 Edremit (Van) earthquakes in Turkey. Eng Fail Anal 2013;34:606–28.
[4] China Building Industry Press. Code for design of concrete structures. GB50010. 2015th ed. Beijing: China Building Industry Press; 2015.
[5] Paulay T, Park R, Priestley MJN. Reinforced concrete beam-column joints under seismic actions. ACI J 1978.
[6] Zhang P, Hou S, Ou J. A beam-column joint element for analysis of reinforced concrete frame structures. Eng Struct 2016;118:125–36.
[7] Tsonos AG, Tegos IA, Penelis GG. Seismic Resistance of Type 2 Exterior Beam-Column Joints Reinforced With Inclined Bars. ACI Struct J 1992;89.
[8] Au FTK, Huang K, Pam HJ. Diagonally-reinforced beam-column joints reinforced under cyclic loading. Struct Build 2005;158:21–40.
[9] Chalioris CE, Favvata MJ, Karayannis CG. Reinforced concrete beam-column joints with crossed inclined bars under cyclic deformations. Earthq Eng Struct Dyn 2008;37:881–97.
[10] Kotsovou G, Mouzakis H. Exterior RC beam-column joints: New design approach. Eng Struct 2012;41:307–19.
[11] Lu X, Urukap TH, Li S, Lin F. Seismic behavior of interior RC beam-column joints with additional bars under cyclic loading. Earthq Struct 2012;3:37–57.
[12] Bindhu KR, Jaya KP. Strength and behaviour of exterior beam column joints with diagonal cross bracing bars. Asian J Civ Eng 2010;11:397–410.
[13] Rajagopal S, Prabavathy S. Investigation on the seismic behavior of exterior beam–column joint using T-type mechanical anchorage with hair-clip bar. J King Saud Univ - Eng Sci 2015;27:142–52.
[14] Bakir PG. Seismic resistance and mechanical behaviour of exterior beam-column joints with crossed inclined bars. Struct Eng Mech 2003;16:493–517.
[15] Chalioris CE, Bantilas KE. Shear strength of reinforced concrete beam-column joints with crossed inclined bars. Eng Struct 2017;140:241–55.
[16] Park R, Milburn JR. Comparison of recent New Zealand and United States seismic design

provisions for reinforced concrete beam-column joints and test results from four units designed according to the New Zealand code. Bull New Zeal Natl Soc Earthq Eng 1983;16:3–24.
[17] Hwang HJ, Eom TS, Park HG. Design considerations for interior RC beam-column joint with additional bars. Eng Struct 2015;98:1–13.
[18] Arowojolu O, Ibrahim A, Rahman MK, Al-Osta M, Al-Gadhib AH. Plastic hinge relocation in reinforced concrete beam–column joint using carbon fiber–reinforced polymer. Adv Struct Eng 2019;22:2951–65.
[19] Maheri MR, Torabi A. Retrofitting external RC beam-column joints of an ordinary MRF through plastic hinge relocation using FRP laminates. Structures 2019;22:65–75.
[20] Wang G, Dai J, Bai Y. Seismic retrofit of exterior RC beam-column joints with bonded CFRP reinforcement: An experimental study. Compos Struct 2019;224:111018.
[21] Senturk M, Pul S, Ilki A, Hajirasouliha I. Development of a monolithic-like precast beam-column moment connection: Experimental and analytical investigation. Eng Struct 2020;205.
[22] Alaee P, Li B, Cheung PPC. Parametric investigation of 3D RC beam-column joint mechanics. Mag Concr Res 2015;67:1054–69.
[23] Al-Osta MA, Khan U, Baluch MH, Rahman MK. Effects of Variation of Axial Load on Seismic Performance of Shear Deficient RC Exterior BCJs. Int J Concr Struct Mater 2018;12.
[24] Li B, Lam ESS, Wu B, Wang YY. Effect of high axial load on seismic behavior of reinforced concrete beam-column joints with and without strengthening. ACI Struct J 2015;112:713–24.
[25] Alaee P, Li B. Analytical Investigations of Reinforced Concrete Beam–Column Joints Constructed Using High-Strength Materials. J Earthq Eng 2020;24:774–802.
[26] Lam ESS, Wu B, Wong YL, Wang ZY, Liu ZQ, Li CS. Drift capacity of rectangular reinforced concrete columns with low lateral confinement and high-axial load. J Struct Eng 2003;129:733–42.